# *IN-SITU* INVETIGATION OF DAMAGE MODE PROGRESSION IN OPEN-HOLE QUASI-ISOTROPIC LAMINATES

Fatih E. Oz[1], Nuri Ersoy[1,2], Mahoor Mehdikhani[3] and Stepan V. Lomov[4]

[1]Department of Mechanical Engineering, Bogazici University, Bebek, 34342, Istanbul, Turkey
[2]Department of Engineering, Design, and Mathematics, University of West England, BS16 1QY, Bristol, United Kingdom
[3-4]Department of Materials Engineering, KU Leuven, Kasteelpark Arenberg 44, 3001 Leuven, Belgium
E-mails: fatih.oz@boun.edu.tr[1], nuri.ersoy@boun.edu.tr[2], mahoor.mehdikhani@kuleuven.be[3], stepan.lomov@kuleuven.be[4]

**Keywords:** Acoustic emission, Digital Image Correlation (DIC), Damage mechanics, Open-Hole Tension, CFRP composites

**Abstract**
In this study, damage mode progression in open-hole (OH) Carbon Fibre Reinforced Polymer (CFRP) laminates are investigated. Two different quasi-isotropic (QI) CFRP laminates are tested with online damage detection techniques. Acoustic Emission (AE) is used primarily for this aim. The k-means++ clustering algorithm is used to group similar AE events. Since the sole application of AE with the clustering algorithm is not sufficient to identify the damage modes, Digital Image Correlation (DIC) and *in-situ* edge microscopy are applied simultaneously, allowing correlating the damage modes and the AE signal characteristics. The lay-up sequence affect the damage mode progression. Transverse cracks in the inner ±45° or 90° plies and micro delaminations at ±45/90 interfaces generate with high frequency and low amplitude events respectively. However the correspondence of high amplitude events varies according to the laminate type: they represent macro delaminations at ±45/90 interfaces in $[-45_2/0_2/+45_2/90_2]_s$ and are surface cracks in $[+45_2/90_2/-45_2/0_2]_s$ laminates.

## 1. Introduction

Presence of a hole causes considerable changes in the mechanical behavior and damage mechanisms in composite laminates. Wisnom and Hallet [1–3] carried out a large experimental and numerical programme to investigate the damage evolution in open-hole tension (OHT) tests of QI Carbon Fibre Reinforced Composites (CFRP) laminates. Change in strength and damage modes in different variants of $[+45_m/90_m/-45_m/0_m]_{ns}$ were investigated with post mortem optical observations. Monitoring the damage during the test using Digital Image Correlation (DIC) allows detecting surface cracks, but is not sufficient for determination of damage in the inner plies of the specimens [4–6]. Nixon-Pearson and Hallett performed post-mortem X-Ray micro-CT analysis at the end of interrupted tests, stopped before final failure, to investigate induced damage after quasi-static tension and tension-tension fatigue tests of $[+45_2/90_2/-45_2/0_2]_s$ laminates [7,8]. Each technique has some drawbacks for reliable detection of damage modes. Recently, Oz et. al. [9,10] applied a multi-instrumental experimental approach to identify the damage modes in different unnotched QI CFRP laminates. 2D DIC and *in-situ* edge microscopy techniques were utilized simultaneously with AE registration during tension tests to identify surface cracks and micro damage modes at inner plies and they were correlated with AE events, clustered with k-means++ clustering algorithm. Robust correlations were attained between the damage modes and the AE characteristics.

In this study, damage mode progression in open-hole (OH) CFRP laminates are investigated using the same multi-instrument methodology: combination of AE, Digital Image Correlation (DIC) and *in-situ*

edge microscopy. Correlations are discovered between the damage at/near surface plies and micro cracks at the inner plies with the corresponding AE characteristics. Transverse cracks in the inner ±45° or 90° plies and micro delaminations at ±45/90 interfaces are always registered with high frequency and low amplitude events respectively. However, the correspondence of high amplitude events vary according to the lay-up of the laminates: they represent macro delaminations at ±45/90 interfaces in $[-45_2/0_2/+45_2/90_2]_s$, and are surface cracks in $[+45_2/90_2/-45_2/0_2]_s$ laminates.

## 2. Material and Experimental Procedure

QI specimens are produced using Hexcel's UD AS4/8552 CFRP prepregs [11]. The fibre volume fraction and nominal thickness of a single ply are 57.4 % and 0.184 mm respectively. Two different variants of QI laminates are tested in this study; a) $[-45_2/0_2/+45_2/90_2]_s$, b) $[+45_2/90_2/-45_2/0_2]_s$. Specimens have 3 mm thickness, 15 mm width, 175 mm length and a central hole with 2.5 mm diameter. Holes are drilled with a carbide drill. OHT tests are performed with electro-mechanical *Instron 4505* universal test machine according to the *ASTM D5766* standard [12] with a rate of 1 mm/min. Two tests for each specimen type are performed until the final failure and five tests are stopped at different stress levels before their ultimate failure: 70%, 80% and 90% of the ultimate tensile strength (UTS). Extensometry is done by 2D DIC.

Vallen AMSY-5 AE system with two broadband Digital Wave B-1025 sensors (frequency range 25-1600 kHz) is used for real time AE registration during tension tests. AE sensors are fixed on the specimens by using C-clamps and they are placed 50 mm away from each other. Only the AE events having amplitudes higher than 45 dB are recorded. A location filter is applied and only events originations from between the two sensors and at least 5 mm away from each sensor are analysed.

Unsupervised k++ means clustering algorithm is used to classify AE events. This algorithm can be summarized as follows. Nine AE features are extracted from an AE event. In the first step, statistically representative features are selected with respect to Laplacian Score and Correlation Coefficient. AE features with higher score and less dependency to others are chosen for the Principal Component Analysis (PCA). It is an orthogonal linear transformation that transforms multidimensional AE data into lower dimension set with a new coordinate system. Then optimal number of clusters is chosen with respect to two evaluation indices. First one is Silhouette Coefficient (SC). Higher SC score means dense and well-separated clusters. Second one is Davies-Bouldin (DB) index which is based on a ratio within-cluster and between cluster distances. Combination of higher SC and lower DB index means better cluster quality. Finally, k-means++ algorithm is used to generate clusters.

LIMESS system, with two high-speed Charge-Coupled Device (CCD) cameras, is used for optical damage detection during tests stopped at 90% UTS. Photo acquisition is done with a rate of 2 photos/second by VIC-Snap software. First camera is used for DIC calculations. A speckle pattern is created on one surface of the specimen for this aim. Second CCD camera uses high magnification lens and it is used for *in-situ* observation of matrix cracks and delaminations in the inner plies in a 5 mm-length frame on free edge of the specimen.

## 3. Results and Discussion

### 3.1. General AE Results

Five tension tests are performed for each laminate type. Figure 1 presents test results for both laminates, combining in one graph stress-strain curve and parameters of the AE events: Amplitude with cumulative AE energy and weighted frequency. Different colours represent different tests. Figure 1 shows that not only stress-strain response, but also the AE results change considerably with the change in lay-up sequence. The maximum stress levels in Figure 1 do not correspond to the ultimate strengths of the specimens, but rather the stress levels that particular tests are stopped.

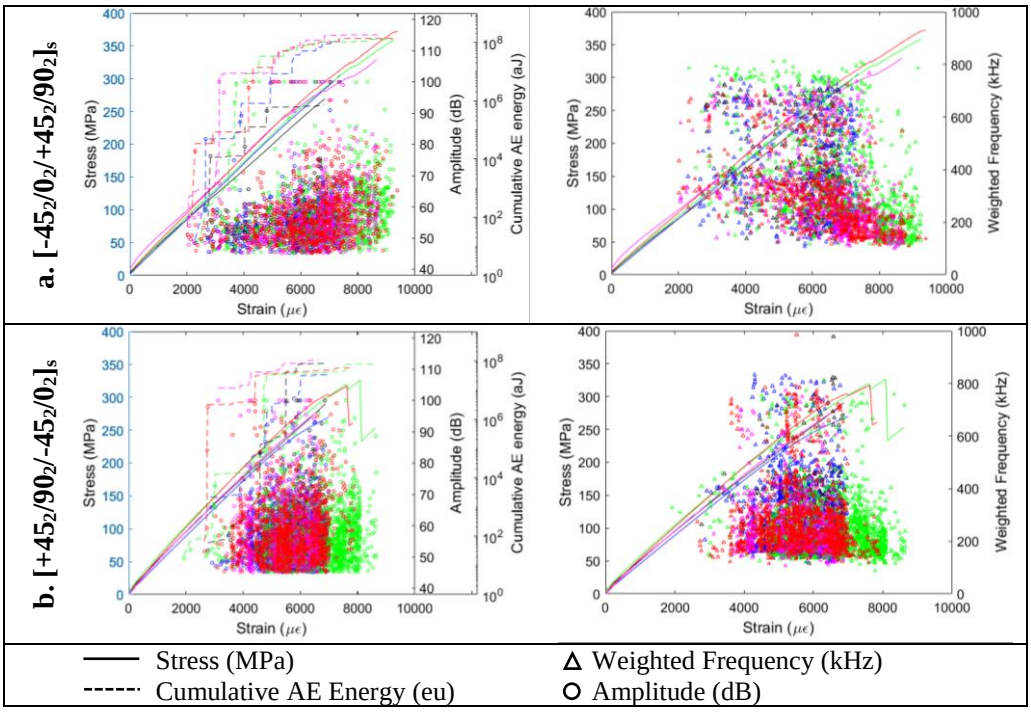


**Figure 1.** Stress-strain curves and AE results for test laminates.

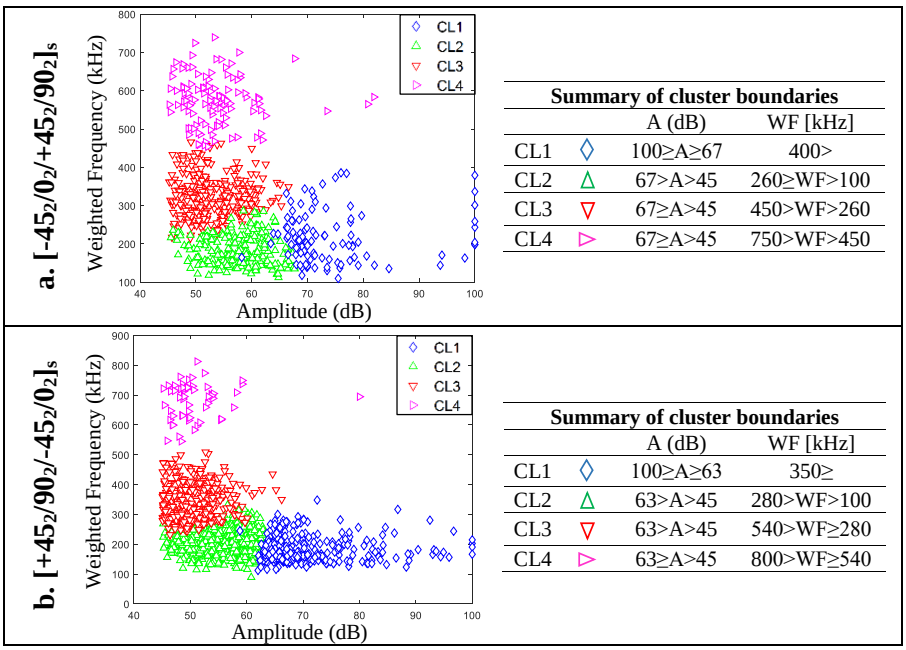


**Summary of cluster boundaries**

| | | A (dB) | WF [kHz] |
|---|---|---|---|
| CL1 | ◇ | 100≥A≥67 | 400> |
| CL2 | △ | 67>A>45 | 260≥WF>100 |
| CL3 | ▽ | 67≥A>45 | 450>WF>260 |
| CL4 | ▷ | 67≥A>45 | 750>WF>450 |

**Summary of cluster boundaries**

| | | A (dB) | WF [kHz] |
|---|---|---|---|
| CL1 | ◇ | 100≥A≥63 | 350≥ |
| CL2 | △ | 63>A>45 | 280>WF>100 |
| CL3 | ▽ | 63>A>45 | 540>WF≥280 |
| CL4 | ▷ | 63≥A>45 | 800>WF≥540 |

**Figure 2.** Summary of cluster groups distribution and their boundaries.

Figure 1.a shows that amplitude and energy levels of registered AE events increase with increasing strain throughout the tests of $[-45_2/0_2/+45_2/90_2]_s$ laminate. At the same time, high weighted frequency events are registered at low strain levels whereas, low weighted frequency events are mostly registered at higher strain levels. Figure 1.b shows that the number of registered AE events reduces considerably after stiffness degradation due to the macro delaminations in $[+45_2/90_2/-45_2/0_2]_s$ laminate at ±45/90 and -45/0 interfaces.

Optimal AE cluster number is found to be four for both laminates as shown in Figure 2. Clusters are well-separated with respect to weighted frequency vs. amplitude parameters. Distribution of cluster

groups and the average values of the boundaries, calculated from the five tests of both laminates are shown in Figure 2.a and Figure 2.b respectively. It is seen that the properties of clusters group for both laminates are very similar but there are small difference between the boundaries of clusters groups of each laminate types. However this does not mean that damage progression is the same in all laminates.

### 3.2. $[-45_2/0_2/+45_2/90_2]_S$

Accumulation of AE events throughout the test is shown in Figure 3.a. Central hole is placed between 21.5 to 24 mm distance to location detecting AE sensor. Edge observation region is around 21 to 26 mm, but due to discrepancy between AE detection and real locations, 20 to 26 mm distance to AE sensor is considered in Figure 3.b. Averaged damage initiation strain level is 2500 με for the five tests since considerable number of events are started to be recorded from this strain level. Presence of a central hole decreases damage initiation level to almost its half from unnotched laminate type (4800 με in unnotched specimens [10]). Accumulation of AE events is as follows: first low-amplitude/high frequency events (CL3-CL4) are registered, then the number of high-amplitude/low-frequency events (CL1) increase considerably through the end of the test for the whole gauge length in Figure 3.a.

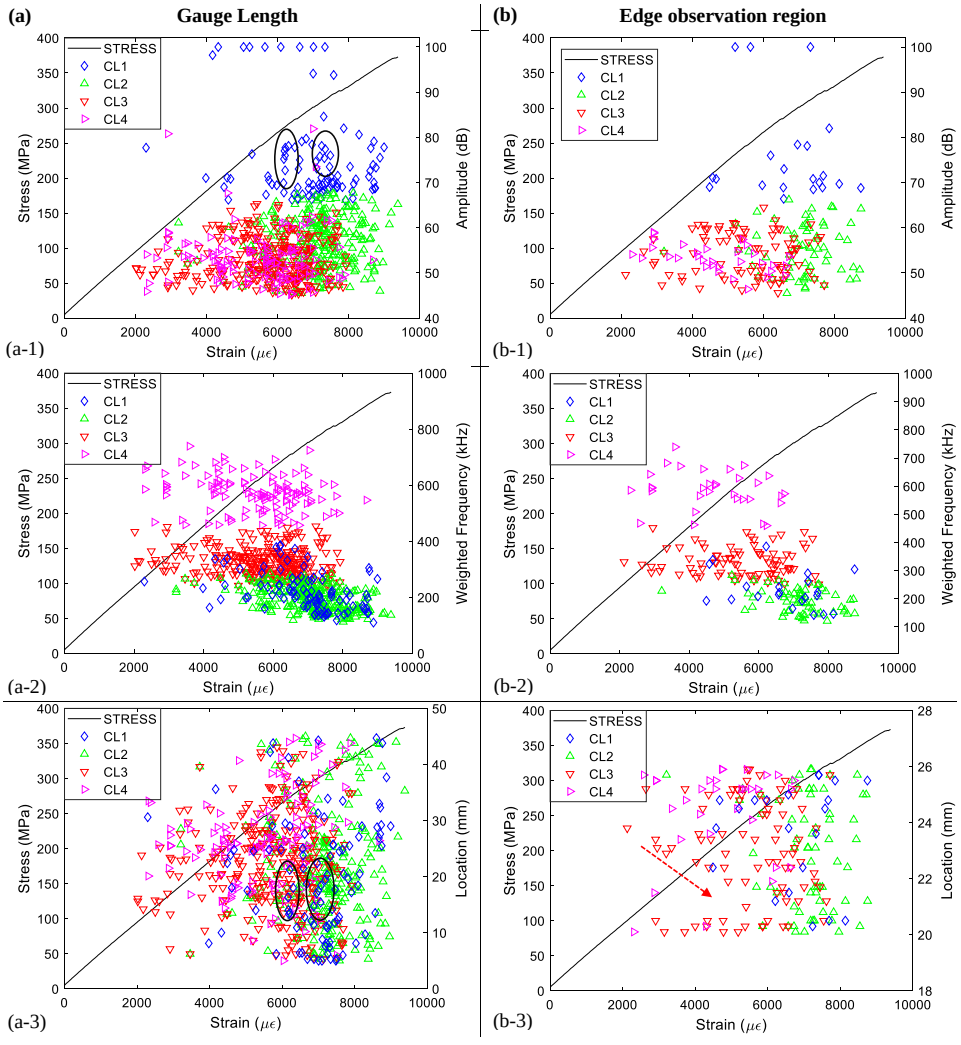


**Figure 3.** Progression of AE clusters throughout a test in $[-45_2/0_2/+45_2/90_2]_s$ laminate: (a) full gage length; (b) edge observation region only

A correlation between AE events in Figure 3 and damage progression in Figure 4 can be done. First damage is observed at 3500 με and it is a transverse crack in mid-90° plies in Figure 4. At this strain level, there are high strained regions are observed in $\varepsilon_1$ strain map along 45° direction in Figure 4. These are transverse cracks in the inner 45° plies. Propagation of transverse cracks are consistent with accumulation of CL4 and CL3 events in Figure 3.

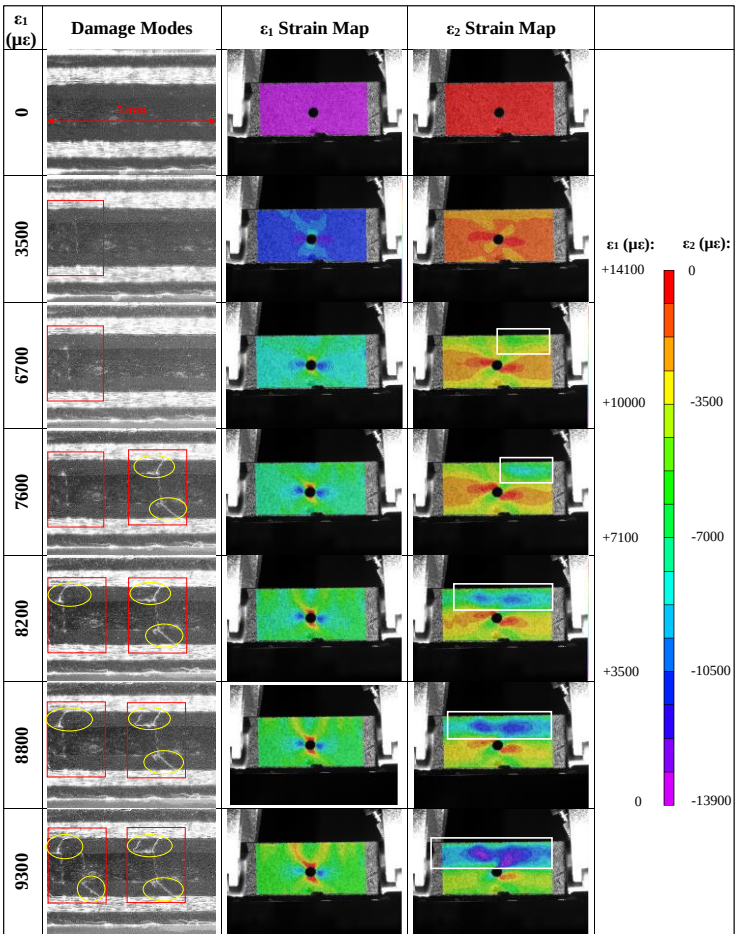


**Figure 4.** Damage detection in $[-45_2/0_2/+45_2/90_2]_s$ laminate via *in-situ* edge microscopy and 2D DIC.

Large contraction in transverse direction ($\varepsilon_2$), due to separation of +45°/90° plies, is shown in white rectangles in Figure 4 (green-blue region at 6700 με – 7600 με and blue-purple regions at higher strain levels in Figure 4). Propagation of macro delamination from 6700 με in Figure 4 is consistent with registration of CL1 in Figure 3.(a-3). The location of delamination initiation is between 5 – 10 mm distance to AE sensor in Figure 3.(a-3). This proves the aforementioned location of delamination initiation and shows its propagation throughout the test. Also, some CL1 events can be seen at 4200 με in Figure 3.b. It is highly possible that these events represent delamination at +45/90 interface around hole region since their locations are between 22 – 24 mm in Figure 3.(a-3). Accumulation of CL1 events from 6200 με until the end of the test can be noticed by tracking the CL1 events in Figure 3.(a-3). It is very consistent with progression of macro delamination in Figure 4. In addition to this damage mode, two surface cracks are seen to occur near the hole at 6100 με and 7100 με. They are not clearly viewed from the DIC strain maps since macro delaminations dominate the strain map and prevents the surface cracks to be observed from the DIC strain maps. These damage modes are registered with high amplitude (CL1) events, as seen in Figure 3.(b-3).

Circled CL1 events in Figure 3 represent surface cracks at the notch tip. Second transverse crack in mid-90° plies occurs with transverse cracks in adjacent +45° plies and with micro delaminations at

their interface at 7600 με in Figure 4. Meanwhile, large contraction in transverse direction at $\varepsilon_2$ strain map becomes more clear at this strain. Number of CL1 events increase rapidly while the registration of CL3-CL4 events almost stops after this strain level of the test, as shown in Figure 3. Because macro delamination becomes the dominant damage mode and propagation of transverse cracks in the inner plies stop after this strain level.

Damage progression and AE registration up to this strain level shows that low-amplitude/high-frequency events (CL4) with low-amplitude/mid-frequency events (CL3) represent damage at inner 90° and +45° plies respectively. Difference between transverse cracks in 90° and +45° plies can be determined by following the propagation of CL3 in Figure 3.(b-3). These events propagate from hole region toward the AE sensor. It is highly possible that these events are transverse cracks in +45° plies whose propagation direction is aligned 45° from the test direction. Thus, it can be said that CL3 events represent damage at the inner +45° plies, while CL4 events are transverse cracks in 90° plies. As proved above, CL1 events represent macro delamination at +45/90 interface mostly. Finally, CL2 represents micro delaminations at 90/+45 interface.

### 3.2. $[+45_2/90_2/-45_2/0_2]_S$

Second laminate type is $[+45_2/90_2/-45_2/0_2]_s$. It is seen (Figure 1.b) that the number of registered events reduce considerably after large load drops due to the macro delaminations at +45/90 and -45/0 interfaces around 7500 με and 8100 με strain levels. Figure 5 shows that damage initiates at 4600 με. High number of AE events with low-amplitude/high-frequency characteristics (CL3) are registered after 4700 με in Figure 5. They are initially localized between 15 – 21 mm in Figure 5.(a-3). They propagate to the hole region after 5100 με, then to the further regions (through 30 mm away from the AE sensor) after 7000 με. High-amplitude events (CL1) are localized around the hole region until 7000 με and propagate to the further regions after 7000 με. Distance of the central hole to the AE sensor is between 23-25.5 mm but location graph for edge observation region is plotted for 21-29 mm in Figure 5.(a-3) because of the quickly propagating long delaminations.

First surface crack next to the hole happens at 4800 με in Figure 6. At the same time, a free edge delamination is detected and shown within white rectangle in the $\varepsilon_2$ strain map in Figure 6. It is highly possible that this free edge delamination occurs due to the transverse cracks in the inner 90° plies. Unfortunately, they are not detected with optical instruments before this strain level. Surface crack propagates to the unobserved edge of the specimen at 5300 με. Meanwhile, the delamination grows at this strain level, approaches to the hole as seen in the white rectangle in Figure 6.

Progression of the surface crack and delamination up to this strain level is consistent with the accumulation of CL1 and CL3 events, clearly seen in Figure 5.a. Early CL3 events are registered between 15-21 mm at 4700 – 5200 με strain levels in Figure 5.(a-3). Then they propagate to the hole region (22-27 mm) after 5200 με. That is consistent with the propagation of delamination, shown within white rectangle, in the $\varepsilon_2$ strain map in Figure 6. Then they accumulate to further regions after 7000 με in Figure 5.(a-3) where delamination regions can be observed on the other side of the hole at this strain level in Figure 6. So, it is highly possible that CL3 events represent macro delaminations at the -45/90 interface. Meanwhile CL1 events are registered due to the cracks on surface +45° plies. It induces next to the hole at 4800 με then propagates to the further regions after 5300 με in Figure 6. This propagation is consistent with the accumulation of CL1 events in Figure 5.(a-3). They are localized at the hole region (between 22-27 mm) and then a quick propagation happens at 5300 με in Figure 5.(a-3). Their propagation through the observed edge of the specimen between 7100 – 7600 με strain levels in Figure 6 can be traced by following the CL1 events between the same interval in Figure 5.(a-3). With the load drop at 7700 με, very few or no CL1 events are registered between 22-28 mm anymore as seen in Figure 5.(b-3) because this surface is already separated near the hole region and it continues to separate near the free edges that is less than 22 mm (at the observed edge) and greater than 28 mm (at the unobserved edge) far from the AE detecting sensor. Thus, it is said that CL1 events represent cracks at the surface +45° plies.

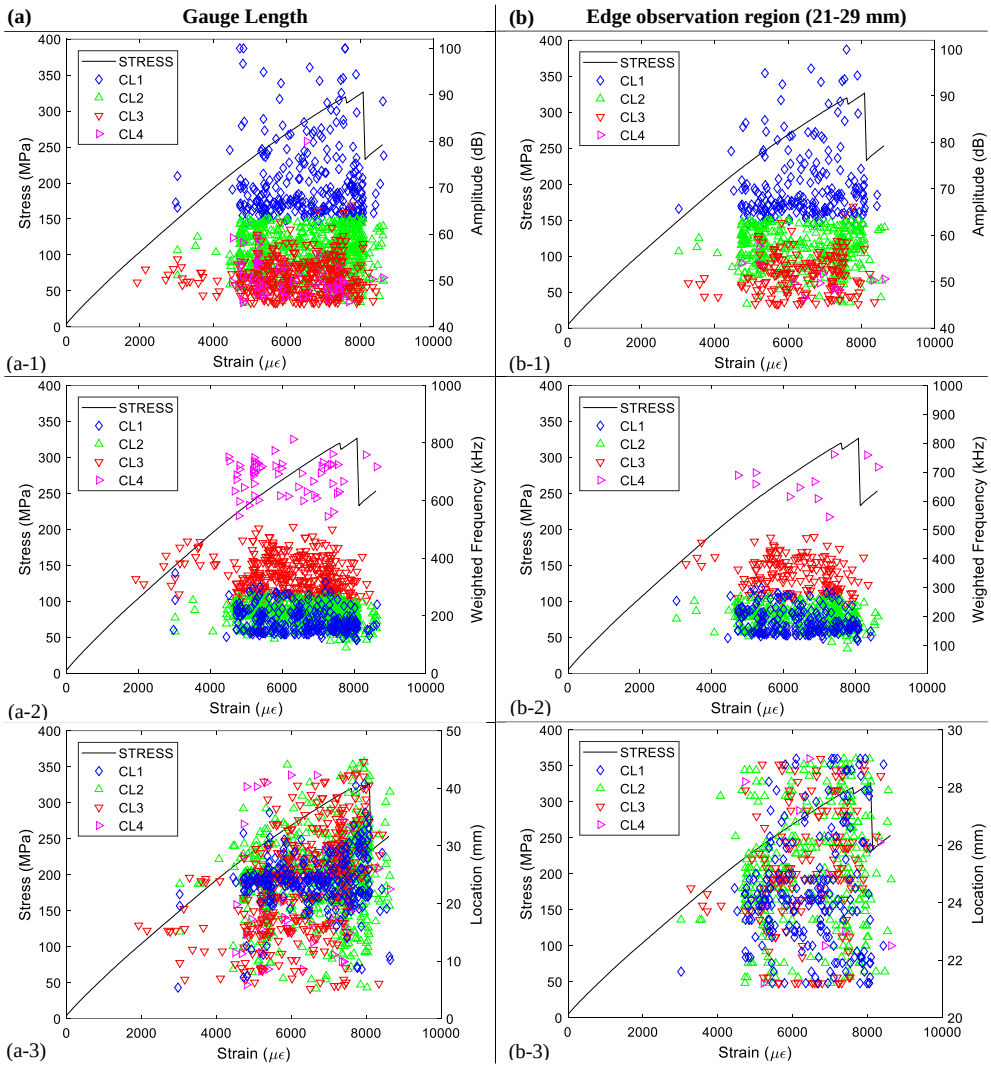


**Figure 5.** Progression of AE clusters throughout a test in $[+45_2/90_2/-45_2/0_2]_s$ laminate: (a) full gage length; (b) edge observation region only

First transverse crack in 90° plies is detected at 7000 με in Figure 6. Immediately after, tip of a delamination at -45/90 interface is observed at 7100 με. Its propagation can be seen until 7600 με in Figure 6. Then it causes transverse cracks in -45° plies at this strain level. Also, the surface crack propagates through the observed edge of the specimen between 7100 – 7600 με in Figure 6. A second transverse crack in 90° plies happens at this strain level. Then, macro delamination separates the upper -45/90 interface in the edge observation region at 7700 με. Moreover, transverse cracks in -45° plies causes delaminations at -45/0 interfaces at 7700 με. Very few CL3 events are registered after this load drop and at further regions as shown in Figure 5.(a-3) since the macro delamination is already propagated to the further region. High-frequency (CL4) events decrease and almost disappear after this load drop too. Thus they represent transverse cracks in the inner plies. It is not easy to distinguish damage at inner 90° and -45° plies. Then, another load drop occurs due to delamination at lower plies at 8100 με. Consequently, the CL1 events disappear with this load drop because surface layer is completely separated as seen in Figure 6. There are two dominant damage modes present in this laminate type. Damage at surface +45° plies (CL1) and macro delamination (CL3). Since these damage modes are considerably large, their presence reduce the sensitivity of AE registration of micro damage modes. Low-amplitude/high-frequency events (CL4) represent transverse cracks both at the inner 90° and -45° plies. Finally, low-amplitude/low-frequency AE events (CL2) represent micro delaminations at ±45/90 interfaces as in $[-45_2/90_2/+45_2/90_2]_s$ laminate.

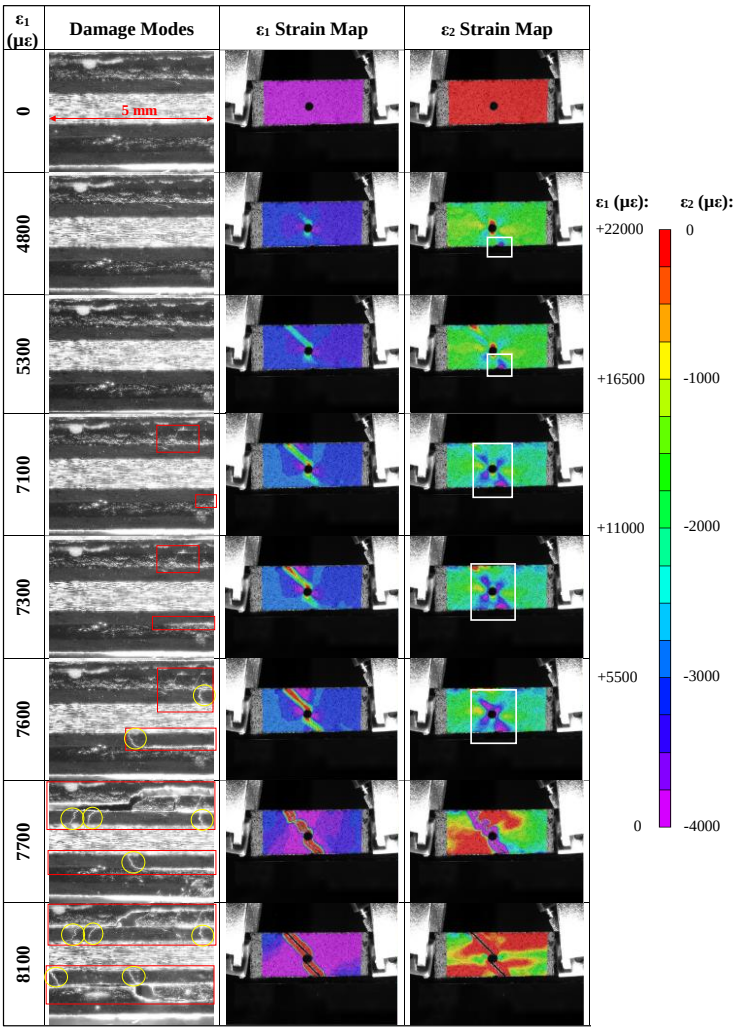


**Figure 6.** Damage progression in $[+45_2/90_2/-45_2/0_2]_s$ laminate.

## 4. Conclusions

Damage progression in OH QI CFRP specimens are investigated in this study. Simultaneously applied 2D DIC and *in-situ* edge microscopy techniques provide to correlate AE clusters with damage modes successfully. Transverse cracks in the inner ±45° or 90° plies and micro delaminations at ±45/90 interfaces are always registered with high frequency and low amplitude events respectively. However the correspondence of high amplitude events vary according to the lay-up of the laminates. While they represent macro delaminations at ±45/90 interfaces in $[-45_2/0_2/+45_2/90_2]_s$, they are surface cracks in $[+45_2/90_2/-45_2/0_2]_s$ laminates. This study provides to see that the damage progression throughout the tests and AE characteristics of damage modes in unnotched and their notched, OH types, are not same. Thus, it can be concluded that presence of a hole does not only cause a change in damage progression but also the AE characteristics of these damage modes.

## Acknowledgments

Authors acknowledge the support of the Boğaziçi University Research Fund, Istanbul Development Agency (ISTKA), and TUBITAK BIDEB 2214-A under project codes 10020/15A06D3, ISTKA/BIL/2012/58 and 1059B141600673 respectively. S.V. Lomov holds the Toray Chair on Composites at KU Leuven, the support of which is gratefully acknowledged.

## References

[1] B. G. Green, M. R. Wisnom, and S. R. Hallett. An experimental investigation into the tensile strength scaling of notched composites. *Composites Part A: Applied Science and Manufacturing*, 38: 867–878, 2007.

[2] M. R. Wisnom and S. R. Hallett. The role of delamination in strength, failure mechanism and hole size effect in open hole tensile tests on quasi-isotropic laminates. *Composites Part A: Applied Science and Manufacturing*, 40: 335–342, 2009.

[3] S. R. Hallett, B. G. Green, W. G. Jiang, and M. R. Wisnom. An experimental and numerical investigation into the damage mechanisms in notched composites. *Composites Part A: Applied Science and Manufacturing*, 40: 613–624, 2009.

[4] G. H. Erçin, P. P. Camanho, J. Xavier, G. Catalanotti, S. Mahdi, and P. Linde. Size effects on the tensile and compressive failure of notched composite laminates. *Composite Structures*, 96: 736–744, Feb. 2013.

[5] B. Aidi and S. W. Case. Experimental and Numerical Analysis of Notched Composites Under Tension Loading. *Applied Composite Materials*, 22: 837–855, 2015.

[6] C. Furtado, A. Arteiro, G. Catalanotti, J. Xavier, and P. P. Camanho. Selective ply-level hybridisation for improved notched response of composite laminates. *Composite Structures*, 145: 1–14, 2016.

[7] O. J. Nixon-pearson, S. R. Hallett, P. J. Withers, and J. Rouse. Damage development in open-hole composite specimens in fatigue. Part 1 : Experimental investigation. *Composite Structures*, 106: 882–889, 2013.

[8] O. J. Nixon-Pearson and S. R. Hallett. An investigation into the damage development and residual strengths of open-hole specimens in fatigue. *Composites Part A: Applied Science and Manufacturing*, 69: 266–278, 2015.

[9] F. E. Oz, N. Ersoy, and S. V. Lomov. Do high frequency Acoustic emission events always represent fibre failure in CFRP laminates?. *Composites Part A: Applied Science and Manufacturing*, 103: 230–235, 2017.

[10] F. E. Oz, N. Ersoy, M. Mehdikhani, and S. V. Lomov. Multi-Instrument *In-situ* Damage Monitoring in Quasi-isotropic CFRP Laminates Under Tension. *Composite Structures*, 2018.

[11] Hexcel. HexPly ® 8552 - Product Data Sheet - EU Version. 1–6, 2016.

[12] ASTM. D5766/5766M: Standard Test Method for Open-Hole Tensile Strength of Polymer Matrix Composite. *Annual Book of ASTM Standards*, 13: 1–7, 2013.